

Local Blockade of Rydberg Excitation in an Ultracold Gas

D. Tong, S.M. Farooqi, J. Stanojevic, S. Krishnan, Y.P. Zhang, R. Côté, E.E. Eyler, and P.L. Gould

Physics Department, University of Connecticut, Storrs, CT 06269

(Dated: October 28, 2018)

In the laser excitation of ultracold atoms to Rydberg states, we observe a dramatic suppression caused by van der Waals interactions. This behavior is interpreted as a local excitation blockade: Rydberg atoms strongly inhibit excitation of their neighbors. We measure suppression, relative to isolated atom excitation, by up to a factor of 6.4. The dependence of this suppression on both laser irradiance and atomic density are in good agreement with a mean-field model. These results are an important step towards using ultracold Rydberg atoms in quantum information processing.

PACS numbers: 32.80.Rm, 03.67.Lx, 34.20.Cf

The possibility of a computer that operates according to the principles of quantum mechanics has attracted growing interest from a variety of research fields [1, 2]. A number of possible implementations are being investigated, including solid-state systems, nuclear magnetic resonance, cavity quantum electrodynamics, trapped dipolar molecules, trapped ions, and trapped neutral atoms. A key element to any successful system is the ability to control the coherent interactions between the fundamental building blocks (qubits). Highly-excited Rydberg atoms with principal quantum numbers $n \gtrsim 30$ have the advantage that they interact quite strongly with each other, allowing information to be exchanged quickly [3]. Here we report an important advance towards using ultracold Rydberg atoms in quantum computing. We observe that the laser excitation of a macroscopic sample of ultracold atoms to high-lying Rydberg states can be dramatically suppressed by their strong long-range interactions. This leads to a local blockade effect, where the excitation of one atom prevents excitation of its neighbors. Our observations agree well with a model based on mean-field interactions.

In a high- n Rydberg state, the electron spends most of its time quite far from the nucleus [4]. As a result, the energy of this highly-excited state is very sensitive to external perturbations, including those caused by neighboring Rydberg atoms. A system of two ultracold Rydberg atoms, subject to these long-range interactions, has been proposed as a possible realization of a quantum logic gate [3, 5]. Rydberg states combine the advantages of long radiative lifetimes and strong long-range interactions, allowing information to be exchanged before decoherence sets in, even when the atoms are sufficiently separated to allow individual addressing. If the atoms are ultracold, they can be highly localized, e.g., in the sites of an optical lattice, allowing control of their interactions and efficient detection of their quantum state. An outstanding challenge is the assurance that at most a single Rydberg atom is produced at a given site. Towards this end, the concept of an excitation blockade has been proposed [6, 7]. With multiple atoms occupying a sufficiently localized site, the strong Rydberg-Rydberg interactions allow at most one

Rydberg excitation. Further excitations are blocked by the large energy level shifts that push the resonant frequencies outside the laser bandwidth.

For two atoms in np states, separated by a distance R , the C_6/R^6 van der Waals (vdW) interaction dominates at long range [8, 9]. The rapid n^{11} scaling of the C_6 coefficient indicates the advantage of using high- n Rydberg states. The original proposals for quantum gates [3] and an excitation blockade [6] with Rydberg atoms involved finite electric fields which mixed the angular momentum states, giving rise to a C_3/R^3 dipole-dipole interaction. The vdW interaction, which we have employed, has the important advantage of providing nonzero energy level shifts for every molecular state regardless of the orientation of the atoms. By contrast, dipole interactions vanish for certain orientations, reducing the efficiency of the dipole blockade mechanism.

The basic idea of the experiment is shown in Fig. 1. We start with a sample of about 10^7 ultracold ^{85}Rb atoms in the $5s$ ground state and illuminate them with a UV pulse resonant with a transition to an np Rydberg state [10]. Once a Rydberg atom is produced, the strong vdW interaction shifts the energy levels of neighboring atoms, suppressing their excitation. As a result, each Rydberg atom resides in a domain, within which no other Rydberg excitation is possible. The higher the atomic density, the more atoms will be in each domain, and the larger will be the factor by which the overall excitation fraction of the macroscopic sample is suppressed. It is this suppression that we observe in the experiment.

The ultracold sample of ^{85}Rb atoms, with a peak density up to 10^{11} cm^{-3} and a temperature of $\sim 100 \mu\text{K}$, is provided by a diode-laser-based vapor-cell magneto-optical trap (MOT). Trapped atoms in a specific hyperfine level of the ground state are excited to $np_{3/2}$ states with $n=30-80$ by a narrowband 297 nm laser pulse of 8.6 ns duration (FWHM), generated by frequency doubling of a pulse-amplified cw laser as in our earlier work [10]. The bandwidth of about 100 MHz, measured by scanning over the $30p$ resonance, is about twice the Fourier transform limit due to frequency chirping in the pulsed amplifier [11]. In order to excite the highest density region,

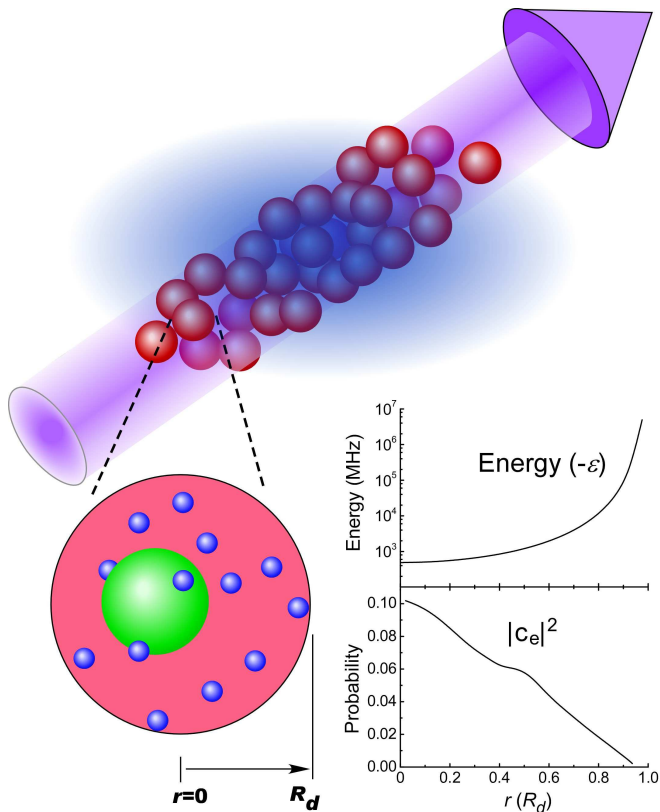


FIG. 1: Schematic of the experiment. Top: a UV laser beam illuminates a sample of ultracold ^{85}Rb atoms in order to excite Rydberg atoms. Our theoretical model divides the region into domains of radius R_d . Zoom: Within a given domain, any one of the numerous ground-state atoms may be excited into a Rydberg state. Inset: Because of strong Rydberg-Rydberg vdW interactions, the mean-field energy shift ε depends on the particular location, as does the excitation probability $|c_e|^2$. Atoms near the domain center are less shifted and their excitation is more probable than those near the periphery. The graphs correspond to $n=80$ atoms at $\rho = 6.5 \times 10^{10} \text{ cm}^{-3}$ and scaled irradiance $I = 0.187 \text{ MW/cm}^2$.

the UV light is focused into the MOT cloud, yielding a cylindrical excitation volume $\sim 500 \mu\text{m}$ long and $\sim 220 \mu\text{m}$ in diameter (FWHM). Within 60 ns after the laser pulse, a $\sim 1500 \text{ V/cm}$ electric field is applied, ionizing the Rydberg atoms and accelerating the ions towards a microchannel plate (MCP) detector. The trapping light is turned off when the UV pulse arrives in order to prevent direct photoionization from the $5p$ level.

The MCP is calibrated using two methods. The first is based on the signal from near-threshold photoionization of the $5s$ ground state. The measured density distribution in the MOT, obtained from the trapped-atom fluorescence profile, is combined with the measured UV beam parameters and the known photoionization cross section [12, 13] to calculate the number of photoions per laser pulse. The second method is based on the $n=30$ Rydberg signal, which behaves as isolated-atom excitation

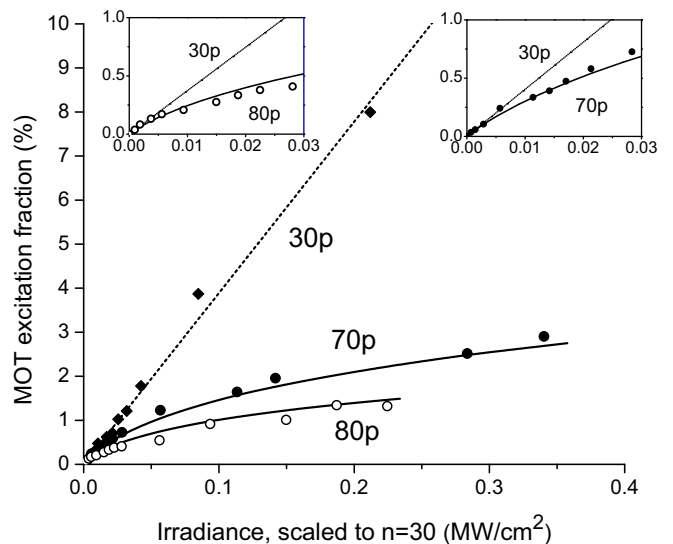


FIG. 2: Comparison of Rydberg excitation for the unblockaded (isolated atom) $30p$ state and the blockaded $70p$ and $80p$ states at a peak density of $6.5 \times 10^{10} \text{ cm}^{-3}$. Irradiance values are scaled by $(n^*/30^*)^3$ to account for the n dependence of the electric dipole transition probability. Insets show the region near the origin with an expanded scale. The dashed line for $n=30$ is a least-squares fit to the data, while the solid curves for $n=70$ and $n=80$ are theoretical predictions, using a single adjustable scaling parameter α as described in the text. To account for the calculated effects of slight variations in the MOT cloud parameters, the $n=30$ results are multiplied by 1.29 ($n=70$ inset), 1.19 ($n=80$ inset) and 1.24 (main figure, using the average correction for $n=70,80$).

at all intensities used, because for $n=30$ the vdW interaction is relatively weak. A linear fit is combined with calculations utilizing the $5s \rightarrow 30p$ oscillator strength of Ref. [14], including the effects of a linear laser frequency chirp corresponding to the observed bandwidth. The two calibrations agree within 2%, confirming that we can make accurate quantitative predictions of excitation probabilities in the absence of a blockade.

The dependence of the Rydberg signal on the peak UV irradiance is shown in Fig. 2 for $n=30, 70$ and 80 . The signal plotted is the fraction of the entire MOT sample that is excited. For each n , the irradiance values are scaled to $n=30$ by the factor $(30^*/n^*)^3$ in order to account for the decrease in transition strength with increasing n . Here $n^*=n-\delta$, and $\delta = 2.6415$ is the quantum defect for $p_{3/2}$ states [15]. Note that the $n=30$ saturation intensity for isolated atoms, defined as that required for an unchirped π -pulse in the center of the beam, is 0.36 MW/cm^2 . With this irradiance scaling, the various n 's would fall on a universal isolated atom excitation curve if the Rydberg levels were unshifted by atomic interactions. This is seen to be the case for the very lowest intensities, at which the Rydberg atoms are sufficiently sparse that interactions between them are negligible.

The salient feature of Fig. 2 is the dramatic suppression of Rydberg excitation for $n=70$ and 80 relative to the isolated atom ($n=30$) excitation curve. As expected, the suppression is larger for $n=80$ due to its stronger vdW interaction, reaching a factor of 6.4 at the highest intensities shown.

We model the suppression of Rydberg excitation by solving the Bloch equations for the ground-state and excited-state amplitudes, c_g and c_e , of a given atom. The key point is to include the energy level shift ε due to interactions with nearby Rydberg atoms. If we consider an $np_{3/2}$ Rydberg atom located at \mathbf{r}_i , labelled $|p_i\rangle$, the first-order shift due to its interaction \hat{V}_{int} with $|p_k\rangle$ is $\varepsilon_{ik} = \langle p_i p_k | \hat{V}_{\text{int}}(\mathbf{r}_i - \mathbf{r}_k) | p_i p_k \rangle$. At large separations, this shift is dominated by the vdW interaction corresponding to a pair of molecular states $^1\Sigma_g^+$ and $^3\Sigma_u^+$, labeled below as $\lambda = 1$ and 2 respectively [8, 9, 10]. For $n=70$, $C_6 = 2.64 \times 10^{22}$ a.u. for both states.

For simplicity, we consider a spherical domain of radius R_d and volume V_d which contains several atoms, but by definition, only a single Rydberg atom $|p_i\rangle$. All other excited atoms, outside the domain, contribute to the total shift of this Rydberg level $\varepsilon_i = \sum_{k \neq i} \varepsilon_{ki}$. The shift of $|p_i\rangle$, and therefore its probability of excitation, depends upon its location within the domain, as shown in the insets to Fig. 1. At the center of the sphere, the distance from any other excited atom is maximized, and the shift is therefore minimized. At the periphery of the domain, the proximity of external Rydberg atoms increases the shift, leading to a stronger suppression of excitation. The domain radius R_d is determined from the condition

$$\rho \int_{V_d} d^3\mathbf{r} |c_e(\mathbf{r}, t)|^2 = 1, \quad (1)$$

where ρ , the local density of atoms, is assumed uniform within the domain. The amplitude $c_e(\mathbf{r}, t)$ of an atom located at \mathbf{r} depends on its shift $\varepsilon(\mathbf{r}, t)$. In our mean-field model, we calculate this shift by replacing the discrete sum by an integral over the excited atoms outside the domain ($V' = V - V_d$) and considering their density $\rho_e(t)$ to be locally uniform:

$$\varepsilon(\mathbf{r}, t) = \rho_e(t) \int_{V'} d^3\mathbf{r}' \frac{-C_6}{|\mathbf{r} - \mathbf{r}'|^6} \sum_{\lambda=1}^2 |\langle p_r p_{r'} | \lambda \rangle|^2. \quad (2)$$

The radius R_d and density ρ_e are related self-consistently via $\rho_e V_d = 1$. The shift of an atom located at $\mathbf{r} = \mathbf{y} R_d$ can be rewritten as

$$\varepsilon(\mathbf{y}, t) = -\tilde{C}_6 g(\mathbf{y}) / R_d^6(t), \quad (3)$$

where the effective vdW coefficient, \tilde{C}_6 , and the spatial variation of the shift, $g(\mathbf{y})$ (with $g(0) = 1$), are obtained by numerical integration of Eq. 2. Substituting

$$R_d^{-3} = \rho \int_{|\mathbf{y}| \leq 1} d^3\mathbf{y} |c_e(\mathbf{y}, t)|^2 \quad (4)$$

into the expression for $\varepsilon(\mathbf{y}, t)$ leads to non-linear Bloch-like equations for the time-dependent amplitudes $c_g(\mathbf{y}, t)$ and $c_e(\mathbf{y}, t)$,

$$i \frac{d}{dt} c_g = \frac{\Omega}{2} e^{i\beta t^2} c_e, \quad (5a)$$

$$i \frac{d}{dt} c_e = -\rho^2 \tilde{C}_6 g \left| \int_{|\mathbf{y}| \leq 1} d^3\mathbf{y} |c_e|^2 \right|^2 c_e + \frac{\Omega}{2} e^{-i\beta t^2} c_g. \quad (5b)$$

Here β characterizes the chirp of the laser pulse and $\Omega(t)$ is the Rabi frequency.

Using the adapted zeroth order wavefunctions for the molecular states $\lambda = 1$ and 2 [9], and averaging over projections m_j of the excited states $|n p_{j=3/2} m_j\rangle$ for atoms outside the domain and integrating over all possible angles of molecular axes, we find $\tilde{C}_6 = 7/60 C_6$. By solving numerically Eqs. 5, we find the local density of excited atoms $\rho_e(\rho, \Omega_0)$ after the Gaussian laser pulse of peak Rabi frequency Ω_0 has ended. To compare with the experimental measurements, this function is averaged over the density and laser intensity profiles in the trapped sample to provide the overall fraction of atoms which is excited. Uncertainties in both ρ and \tilde{C}_6 are taken into account by using the scaling factor defined via $\rho_\alpha \tilde{C}_{6,\alpha}^{1/2} = \alpha \rho \tilde{C}_6^{1/2}$.

The data and the predictions of the model described above are compared in Fig. 2 for both $n=70$ and $n=80$. We limit the scaled irradiance to less than 0.35 MW/cm² because the validity of the model is questionable when the isolated atom excitation approaches saturation. For the curves shown, we have used a scaling factor $\alpha=2.4$. This reflects a possible underestimate of the absolute atomic density ρ (known only to within a factor of two) and/or the effective C_6 coefficient. With this scaling factor, the agreement between the model and the data is quite good. For $n=80$, we observe a maximum overall suppression by a factor of 6.4 relative to isolated atom excitation, and the theory indicates the suppression reaches a factor of 19 in the center of the MOT.

We have also measured the excitation fraction as a function of atomic density at a fixed laser irradiance. The density is varied by transiently transferring the population between the two hyperfine levels of the ground state, $F=2$ and $F=3$, which are separated by 3.0 GHz. Since our UV laser bandwidth is very narrow, it excites selectively from only one of these levels. Therefore, changing their relative population immediately preceding the UV pulse, while keeping other parameters of the MOT fixed, varies the effective atomic density available for excitation. This population transfer is due to the slow ($\sim 100 \mu\text{s}$) optical pumping into $F=2$ which occurs when the repumping laser is turned off before the trapping laser. The extent of the transfer is controlled by the time interval between switching off these two lasers. The effective

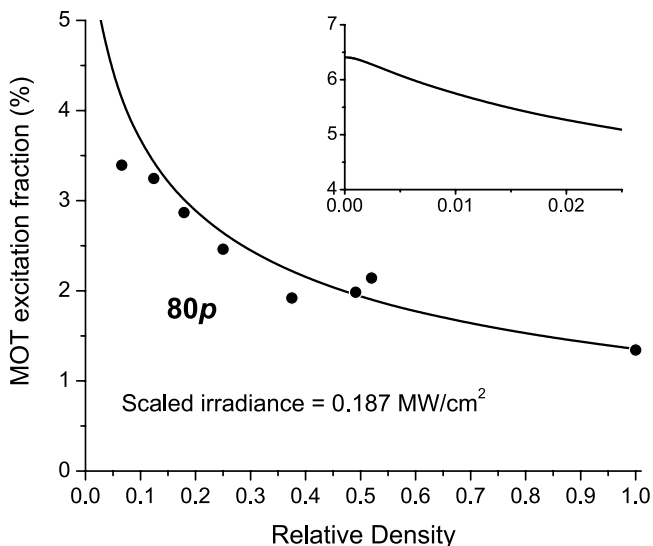


FIG. 3: Density dependence of the $n=80$ Rydberg signal. Relative densities are accurate to 5-10%, but the absolute peak density, nominally $6.5 \times 10^{10} \text{ cm}^{-3}$ at a relative density of 1.0, is uncertain by as much as a factor of two. MOT fractions are expressed in terms of the available ground-state population in the selected hyperfine level (see text). The solid curve shows the mean-field theoretical prediction, using the same scaling parameter as for Fig. 2.

density is measured by comparing the isolated atom signals from $F=2$ and $F=3$ to the $n=30$ state.

The measured excitation fraction for $n=80$ as a function of atomic density is shown in Fig. 3 along with the prediction of the model. Note that the excitation fraction is with respect to the number of atoms in the appropriate hyperfine level. The scaling factor in the model is again chosen to be $\alpha=2.4$. Just as for the irradiance dependence in Fig. 2, the data and the model agree quite well. Note that in the absence of a blockade, one would expect a constant excitation fraction (here 6.4%) instead of the rapid decrease observed.

We have verified that the suppression of excitation we have observed is not due to Stark shifts from charges created during the UV laser pulse. At sufficiently high intensities, we do observe significant numbers of free electrons within 30 ns of a resonant excitation pulse. However, at the maximum irradiance used in the present work, 5.1 MW/cm^2 for $n=80$, we observe less than 100 such electrons. In the worst case, if these electrons were all produced during the laser pulse, the resulting average microfield would be less than 20 mV/cm. If all were to leave the excitation volume, the space charge field at its edge would be ~ 50 mV/cm. The resulting Stark shifts for $80p$ are 0.9 MHz and 5.6 MHz, respectively, negligible compared to the laser bandwidth of ~ 100 MHz.

In conclusion, we have observed a local blockade of Rydberg state excitation in a macroscopic sample due

to strong vdW interactions. The dependence of this dramatic suppression on laser irradiance, atomic density, and principal quantum number are in good agreement with a model based on a mean-field treatment of the atomic interactions. We have observed a sample-averaged suppression by up to a factor of 6.4 relative to isolated atom excitation. Increasing the atomic density should result in significantly larger suppressions. The prospects of achieving a complete blockade in a microscopic sample, such as at a single site in an optical lattice, look very promising. For example, with a density of 10^{12} cm^{-3} and a laser bandwidth of 1 MHz, we conservatively estimate that in a spherical sample of 50 atoms, the probability of exciting more than one atom to $n=80$ is less than 1%. This would represent another important step toward quantum computing with ultracold Rydberg atoms.

This work was supported by the University of Connecticut Research Foundation, the Research Corporation, and grants PHY-998776 and ITR-0082913 from the National Science Foundation.

-
- [1] C. Macchiavello, G.M. Palma, and A. Zeilinger (editors), *Quantum Computation and Quantum Information Theory* (World Scientific, Singapore, 2000).
 - [2] M.A. Nielsen and I.L. Chuang, *Quantum Computation and Quantum Information* (Cambridge University Press, Cambridge, 2000).
 - [3] D. Jaksch, J.I. Cirac, P. Zoller, S.L. Rolston, R. Côté, and M.D. Lukin, *Phys. Rev. Lett.* **85**, 2208 (2000).
 - [4] T.F. Gallagher, *Rydberg Atoms* (Cambridge University Press, Cambridge, 1994).
 - [5] I.E. Protsenko, G. Reymond, N. Schlosser, and P. Grangier, *Phys. Rev. A* **65**, 052301 (2002).
 - [6] M.D. Lukin, M. Fleischhauer, R. Côté, L.M. Duan, D. Jaksch, J.I. Cirac, and P. Zoller, *Phys. Rev. Lett.* **87**, 037901 (2001).
 - [7] M. Saffman and T.G. Walker, *Phys. Rev. A* **66**, 065403 (2002).
 - [8] C. Boisseau, I. Simboten, and R. Côté, *Phys. Rev. Lett.* **88**, 133004 (2002).
 - [9] M. Marinescu, *Phys. Rev. A* **56**, 4764 (1997).
 - [10] S.M. Farooqi, D. Tong, S. Krishnan, J. Stanojevic, Y.P. Zhang, J.R. Ensher, A.S. Estrin, C. Boisseau, R. Côté, E.E. Eyler, and P.L. Gould, *Phys. Rev. Lett.* **91**, 183002 (2003).
 - [11] N. Melikechi, S. Gangopadhyay, and E.E. Eyler, *J. Opt. Soc. Am. B* **11**, 2402 (1994).
 - [12] G.V. Marr and D.M. Creek, *Proc. Roy. Soc. A* **304**, 233 (1968).
 - [13] D. Ciampini, M. Anderlini, J.H. Muller, F. Fuso, O. Morsch, J.W. Thomsen, and E. Arimondo, *Phys. Rev. A* **66**, 043409 (2002).
 - [14] L.N. Shabanova and A.N. Khlyustalov, *Opt. Spectrosc. (USSR)* **56**, 128 (1984).
 - [15] C.J. Lorenzen and K. Niemax, *Phys. Scr.* **27**, 300 (1983).